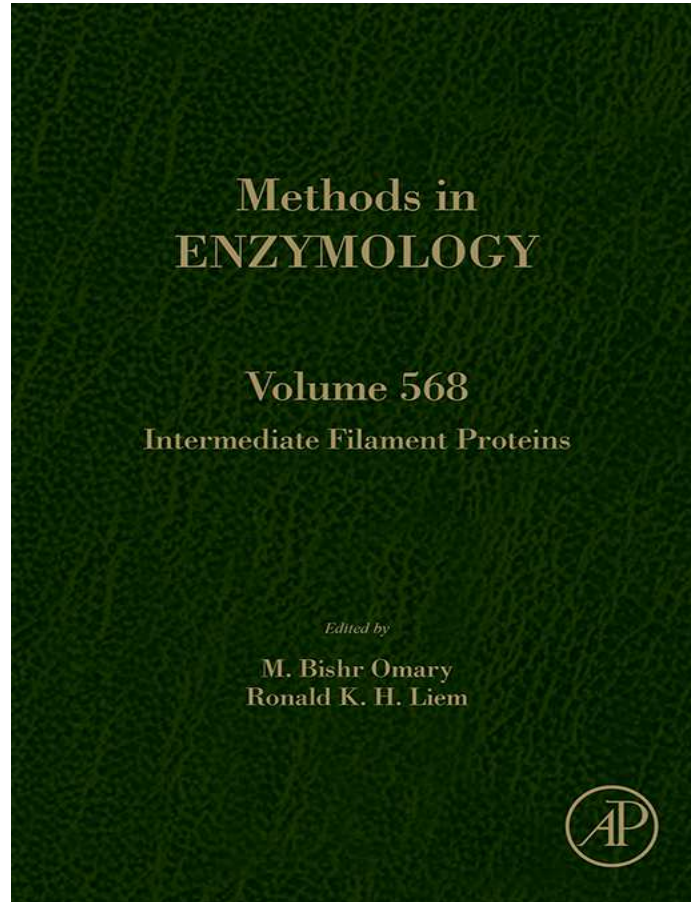


**Provided for non-commercial research and educational use only.
Not for reproduction, distribution or commercial use.**

This chapter was originally published in the book *Methods in Enzymology*, Vol. 568 published by Elsevier, and the attached copy is provided by Elsevier for the author's benefit and for the benefit of the author's institution, for non-commercial research and educational use including without limitation use in instruction at your institution, sending it to specific colleagues who know you, and providing a copy to your institution's administrator.



All other uses, reproduction and distribution, including without limitation commercial reprints, selling or licensing copies or access, or posting on open internet sites, your personal or institution's website or repository, are prohibited. For exceptions, permission may be sought for such use through Elsevier's permissions site at:

<http://www.elsevier.com/locate/permissionusematerial>

From Oliver Jahnel, Bernd Hoffmann, Rudolf Merkel, Olaf Bossinger and Rudolf E. Leube, Mechanical Probing of the Intermediate Filament-Rich *Caenorhabditis Elegans* Intestine. In: M. Bishr Omary and Ronald K.H. Liem, editors, *Methods in Enzymology*, Vol. 568, Burlington: Academic Press, 2016, pp. 681-706.

ISBN: 978-0-12-803470-5

© Copyright 2016 Elsevier Inc.

Academic Press



Mechanical Probing of the Intermediate Filament-Rich *Caenorhabditis Elegans* Intestine

Oliver Jahnel^{*}, Bernd Hoffmann[†], Rudolf Merkel[†], Olaf Bossinger^{*,1},
Rudolf E. Leube^{*,2}

^{*}Institute of Molecular and Cellular Anatomy, RWTH Aachen University, Aachen, Germany

[†]Institute of Complex Systems, ICS-7: Biomechanics, Jülich, Germany

²Corresponding author: e-mail address: rleube@ukaachen.de

Contents

| | |
|--|-----|
| 1. Introduction | 682 |
| 2. Imaging of Intermediate Filaments in <i>C. elegans</i> Intestines by Epifluorescence Microscopy | 686 |
| 3. Outline of Intestinal Rings in <i>C. elegans</i> by a Fluorescent Apical Junction Reporter | 688 |
| 3.1 Confocal Laser Scanning Microscopy of Worms | 690 |
| 4. Dissection of Intestines and Vitality Testing | 691 |
| 4.1 Viability Testing of the Dissected Intestine | 691 |
| 5. Experimental Setup for Micropipette Measurements | 695 |
| 5.1 Forging of Pipettes | 696 |
| 5.2 Calibrating Pipette Setup | 697 |
| 5.3 Analysis of Intestinal Mechanics | 699 |
| 6. Outlook | 702 |
| Acknowledgments | 703 |
| References | 703 |

Abstract

It is commonly accepted that intermediate filaments have an important mechanical function. This function relies not only on intrinsic material properties but is also determined by dynamic interactions with other cytoskeletal filament systems, distinct cell adhesion sites, and cellular organelles which are fine-tuned by multiple signaling pathways. While aspects of these properties and processes can be studied *in vitro*, their full complexity can only be understood in a viable tissue context. Yet, suitable and easily accessible model systems for monitoring tissue mechanics at high precision are rare. We show that the dissected intestine of the genetic model organism *Caenorhabditis elegans* fulfills this requirement. The 20 intestinal cells, which are arranged in an invariant

¹ Current address: Molecular Cell Biology, Institute of Anatomy I, University of Cologne, 50937 Cologne, Germany.

fashion, are characterized by a dense subapical mesh of intermediate filaments that are attached to the *C. elegans* apical junction. We present procedures to visualize details of the characteristic intermediate filament–junctional complex arrangement in living animals. We then report on methods to prepare intestines with a fully intact intermediate filament cytoskeleton and detail procedures to assess their viability. A dual micropipette assay is described to measure mechanical properties of the dissected intestine while monitoring the spatial arrangement of the intermediate filament system. Advantages of this approach are (i) the high reproducibility of measurements because of the uniform architecture of the intestine and (ii) the high degree of accessibility allowing not only mechanical manipulation of an intact tissue but also control of culture medium composition and addition of drugs as well as visualization of cell structures. With this method, examination of worms carrying mutations in the intermediate filament system, its interacting partners and its regulators will become feasible.

ABBREVIATIONS

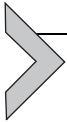
C. elegans *Caenorhabditis elegans*

CeAJ *C. elegans* apical junction

CFP cyan fluorescent protein

int intestinal ring

PBS phosphate-buffered saline



1. INTRODUCTION

Cells experience a wide range of mechanical stresses in their native tissue environment. This is especially true for epithelial cells, which are responsible for efficient and continuous barrier formation while being subjected to forces from the outside and inside of the body. Major players in the integration and dissipation of these forces are the intermediate filaments together with their plasma membrane attachment sites by acting as mechanical shock absorbers, especially at large deformations (Beil et al., 2003; Fudge et al., 2008). The *in vitro* observations, that single-intermediate filaments can be stretched up to 3.6-fold before breaking (Kreplak, Bär, Letierrier, Herrmann, & Aebi, 2005) and that intermediate filaments respond to high strains by hardening (e.g., Janmey, Euteneuer, Traub, & Schliwa, 1991; Lin et al., 2010), are ideal properties to support this function. Observations on genetically modified cells provide further evidence. Thus, deletion of vimentin intermediate filaments leads to reduced stiffness and impaired mechanical stability of fibroblasts resulting in reduced migration and contraction (Brown, Hallam, Colucci-Guyon, & Shaw, 2001; Eckes et al., 1998; Wang & Stamenović, 2000). Expression of different desmin intermediate filament mutants in rat fibroblasts leads to altered cell stiffness

as determined by atomic force microscopy (Plodinec et al., 2011). Similarly, epithelial cells expressing keratin mutants (Lulevich, Yang, Rivkah Isseroff, & Liu, 2010) and keratin-free keratinocytes are less stiff but become more motile (Ramms et al., 2013; Seltmann, Fritsch, Kas, & Magin, 2013; Seltmann, Roth, et al., 2013). The occurrence of blister-forming diseases in patients carrying point mutations in keratin genes is probably the most compelling evidence for a mechanical function of epithelial intermediate filaments (recent review in Homberg & Magin, 2014). However, the underlying mechanisms are still not fully understood. Besides a direct mechanical contribution of keratin filaments themselves, perturbed signaling and adhesion are also considered to be important factors in the development of mechanical deficiencies (Kröger et al., 2013; Liovic et al., 2008; Russell, Ross, & Lane, 2010; Seltmann, Cheng, Wiche, Eriksson, & Magin, 2015).

In the recent past considerable efforts have been undertaken to measure mechanical properties of the cellular intermediate filament system. Most emphasis has been on the investigation of single cells using microchannels (Rolli, Seufferlein, Kemkemer, & Spatz, 2010), microfluidic optical stretchers (Seltmann, Fritsch, et al., 2013), and atomic force microscopy (Lulevich et al., 2010; Ramms et al., 2013; Walter, Busch, Seufferlein, & Spatz, 2011) to probe whole-cell mechanical properties from the outside, while particle-tracking microrheology (Sivaramakrishnan, DeGiulio, Lorand, Goldman, & Ridge, 2008) and magnetic tweezers (Ramms et al., 2013) have been used for testing cytoplasmic viscoelasticity. These studies were complemented by analyses of the keratin cytoskeleton in fixed and partially extracted cells (e.g., Beil et al., 2003; Paust, Paschke, Beil, & Marti, 2013; Walter et al., 2011). Besides encountering a very high degree of cell-to-cell variability, these analyses neglected the tight coupling of epithelial cells to each other and the extracellular matrix. For epithelial cell sheets, analyses have been restricted to reconstituted cell monolayers using disperse assays to examine tissue cohesion (Kröger et al., 2013) and to the study of keratin network dynamics in cells grown on flexible substrates (Beriault et al., 2012; Felder et al., 2008; Fois et al., 2013; Fudge et al., 2008; Hecht et al., 2012).

Thus, a major current need is the investigation of the mechanical properties of the epithelial intermediate filament cytoskeleton in its native tissue environment. Such an enterprise should taken into account the multidimensional intermediate filament network organization, which is determined by its cell type-specific 3D arrangement, turnover dynamics, association with other filament systems, attachment to defined adhesion

sites, and the multiple dynamic interactions with other cellular components. The complex nature of vertebrate tissues and the substantial efforts needed to isolate, cultivate, and genetically modify them are major obstacles. Therefore, using the genetic model organism *Caenorhabditis elegans* may offer a simplified approach. Its highly invariant body plan, the simplicity and speed to grow and propagate clonal worm lines and the easiness of genetic manipulation together with the abundance of intermediate filaments in the epithelial tissues of *C. elegans* are all in favor of using this very well-characterized model organism. A proof of principle was recently provided by the elegant work of Michel Labouesse and his group which uncovered an epidermal mechanotransduction pathway in the epidermis resulting in intermediate filament phosphorylation (Zhang et al., 2011). Remarkably, they were able to show that application of mechanical pressure on *C. elegans* embryos can trigger this pathway. Our own interest is in the epithelial cytoskeleton of the *C. elegans* intestine (Carberry et al., 2012; Carberry, Wiesenfahrt, Windoffer, Bossinger, & Leube, 2009). The approximately 800 μm long tube-like intestine (midgut) extends from the pharynx (foregut) to the hindgut and consists of 20 cells, which are involved in nutrient uptake and secretion. They are arranged as a single-cell layer forming nine intestinal rings (ints) surrounding the ellipsoid lumen (recent review in McGhee, 2013).

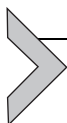
The *C. elegans* genome contains 11 cytoplasmic intermediate filament genes coding for at least 14 polypeptides because of differential splicing (Carberry et al., 2009; Dodemont, Riemer, Ledger, & Weber, 1994; Karabinos, Schmidt, Harborth, Schnabel, & Weber, 2001) and a single gene for a nuclear lamin (Gruenbaum, Lee, Liu, Cohen, & Wilson, 2002; Liu et al., 2000). Of the 11 genes encoding cytoplasmic intermediate filament polypeptides, six are predominantly if not exclusively transcribed in the intestine. They encode for IFB-2, IFC-1, IFC-2, IFD-1, IFD-2, and IFP-1 (Carberry et al., 2009). All are characterized by a central α -helical rod domain with subdomains L1, L12, and L2 encompassing the characteristic heptad repeat needed to form the stable coiled-coil dimers (Carberry et al., 2009; Dodemont et al., 1994). The polymerization properties of the intestinal intermediate filaments have not been investigated to date. A unique feature of the cytoplasmic *C. elegans* intermediate filament polypeptides is the presence of a 42 amino acid insertion in coil 1b that is typical for protostomia and the nuclear lamins. The B-type intermediate filament polypeptides also contain an Ig-like domain in their carboxytermini. Evolutionary analyses show that the intestinal intermediate filament polypeptides of *C. elegans* are unique and differ from those expressed in other nematodes, invertebrates, and vertebrates (Table 1).

Table 1 OrthoMCL Clusters of *C. elegans* Intestinal Intermediate Filaments, *C. elegans* Intermediate Filaments in Other Tissues and *C. elegans* Lamin (in Cooperation with P. Schiffer, Biocenter University of Cologne)

| | | IFB-2 (intestine) | IFC-1 (intestine) | IFC-2 (intestine) | IFD-1 (intestine) | IFD-2 (intestine) | IFP-1 (intestine) | IFA-1/MUA-6/ IFA-3/IFA-4/IFB-1 (other tissues) | LMN-1 (lamin) |
|-------------------|-----------------------|------------------------|-------------------|-------------------|-------------------|-------------------|-------------------|--|---------------|
| Nematoda (clades) | V | <i>C. elegans</i> | 1 | 1 | 1 | 1 | 1 | 5 | 1 |
| | V | <i>C. briggsae</i> | 1 | 1 | 1 | 1 | 1 | 5 | 1 |
| | V | <i>C. remanei</i> | 1 | 1 | 1 | 1 | 1 | 5 | 1 |
| | V | <i>C. angaria</i> | 1 | - | - | 1 | - | 4 | 2 |
| | V | <i>P. pacificus</i> | - | - | - | - | - | 5 | 1 |
| | IV | <i>B. xylophilus</i> | - | - | - | - | - | 4 | 1 |
| | IV | <i>M. hapla</i> | - | - | - | - | - | 1 | 1 |
| | III | <i>D. immitis</i> | - | - | - | - | - | 4 | 1 |
| | III | <i>L. loa</i> | - | - | - | - | - | 4 | 1 |
| | III | <i>A. suum</i> | - | - | - | - | - | 3 | 1 |
| | III | <i>B. malayi</i> | - | - | - | - | - | 3 | 1 |
| | II | <i>E. brevis</i> | - | - | - | - | - | 1 | 2 |
| I | <i>T. spiralis</i> | - | - | - | - | - | 2 | 1 | |
| I | <i>R. culicivoxax</i> | - | - | - | - | - | 1 | 1 | |
| Other species | Nematomorpha | <i>Gordius spec.</i> | - | - | - | - | - | 3 | 3 |
| | Tardigrada | <i>H. dujardini</i> | - | - | - | - | - | - | 3 |
| | Hexapoda | <i>D. melanogaster</i> | - | - | - | - | - | - | 2 |
| | Hexapoda | <i>A. pisum</i> | - | - | - | - | - | - | 2 |
| | Hexapoda | <i>T. castaneum</i> | - | - | - | - | - | - | 1 |
| | Chelicerata | <i>T. urticae</i> | - | - | - | - | - | - | 1 |
| | Lophotrochozoa | <i>C. capitata</i> | - | - | - | - | - | - | 1 |
| | Crustacea | <i>D. pulex</i> | - | - | - | - | - | - | 1 |
| | Myriapoda | <i>S. maritima</i> | - | - | - | - | - | - | 1 |
| | Echinodermata | <i>S. purpuratus</i> | - | - | - | - | - | - | 1 |
| | Chordata | <i>B. floridae</i> | - | - | - | - | - | - | 1 |
| Vertebrata | <i>H. sapiens</i> | - | - | - | - | - | - | 3 | |

The presence of the *C. elegans* intestinal intermediate filaments seems to be linked to the endotube, a prominent and mechanically resilient structure that is characteristic for *C. elegans*. The endotube is a clearly discernable dense region in electron micrographs, which is located just below the organelle-free terminal web that anchors the microvillar actin bundles (Bossinger, Fukushige, Claeys, Borgonie, & McGhee, 2004; McGhee, 2013; Munn & Greenwood, 1984). The intestinal intermediate filaments are highly enriched in the subapical region and have been localized to the endotube by immunoelectron microscopy (Bossinger et al., 2004). The endotube is anchored to the *C. elegans* apical junction (CeAJ). This apical cell–cell adhesion site is ultrastructurally homogenous but encompasses several molecular subdomains (recent review in Pásti & Labouesse, 2014).

In this communication, we will first describe, how the intermediate filaments and cell junctions are organized as a contiguous sheath surrounding the intestinal lumen and will then go on to describe a simple method to isolate functionally intact intestines, whose mechanical properties can be quantitatively examined using a dual pipette assay. Possible applications of this system will be briefly outlined at the end.



2. IMAGING OF INTERMEDIATE FILAMENTS IN *C. elegans* INTESTINES BY EPIFLUORESCENCE MICROSCOPY

The following protocol is routinely used to examine the intermediate filament distribution in worms producing fluorescently labeled reporters. Figure 1 shows a live L4 larva, in which IFB-2::CFP fusion proteins localize specifically to the subapical periluminal domain of the intestine (Carberry et al., 2009; Hüskén et al., 2008). The continuous tube-like sleeve surrounding the intestinal lumen from the first to ninth int is readily seen.

Materials

- Viable L4 larvae of strain BJ49 *kcl56 [ifb2::cfp]IV*
- Levamisole (Sigma–Aldrich, cat no. 31742)
- 2.5% (w/v) agarose (Biozym, cat no. 840004) in distilled H₂O
- Microscope slides (e.g., Menzel–Gläser, cat no. cut edges AA00000102E)
- Vaseline
- Platinum wire (VWR, cat no. 631-7101) to prepare a worm pick
- Phosphate-buffered saline (PBS; Sigma–Aldrich, cat no. D8537)

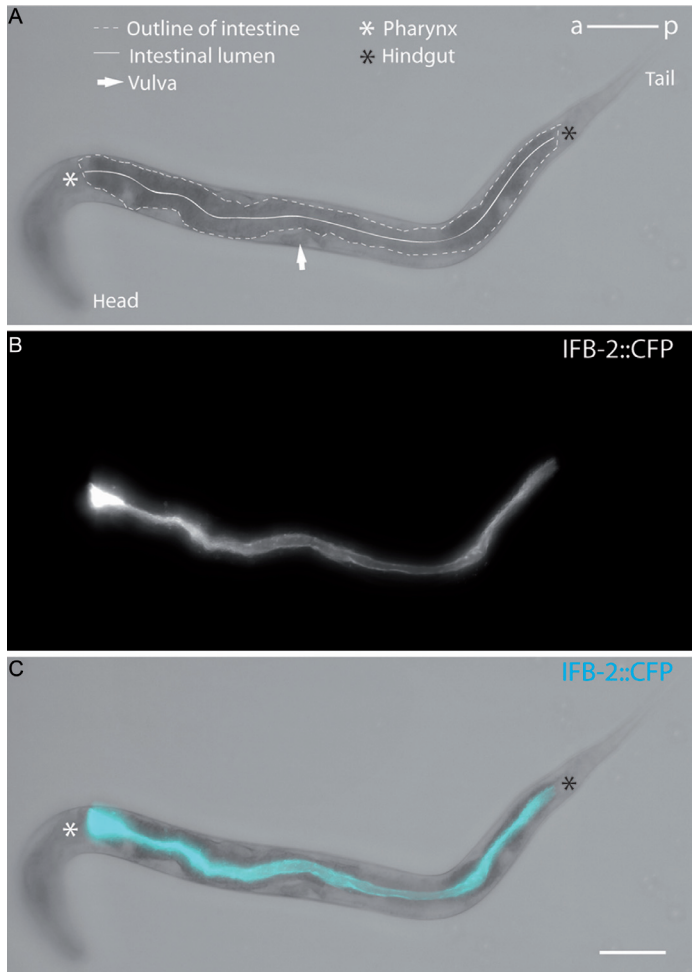


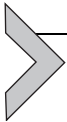
Figure 1 Fluorescence distribution of an IFB-2::CFP reporter in an L4 larva of strain BJ49. The fluorescence is concentrated in a dense network in the apical cytoplasm of intestinal cells entirely surrounding the intestinal lumen. (A) Phase-contrast micrograph, (B) corresponding fluorescence micrograph and merged overlay with fluorescence in cyan (light gray in the print version) in (C). The fluorescence signal is restricted to the intestine beginning after the pharyngeal terminal bulb (white asterisk) and ending before the hindgut (black asterisk). The dashed line shows the contours of the intestinal cells, the continuous line shows the position of the intestinal lumen. Arrow, vulva; a, anterior; p, posterior. Scale bar: 50 μ m.

Equipment

- Fluorescence microscope (e.g., Zeiss ApoTome 2, Carl Zeiss)
- 20× Objective (e.g., Plan-Apochromat 20×/0.8 M27, Carl Zeiss)

Methods

1. To prepare agarose pads, melt the 2.5% agarose solution and place a drop between two microscope slides to flatten. After hardening, slides are separated and the pad adhering to one of the slides is ready for use.
2. Transfer L4 larvae with the worm pick into a 20- μ l drop of PBS containing 1 mM Levamisole that had been placed on the agarose pad. Put a coverslip on top and ensure that all edges of the coverslip are completely sealed with vaseline to prevent evaporation.
3. Record phase-contrast images and IFB-2::CFP fluorescence using the CFP (cyan fluorescent protein) filter set.



3. OUTLINE OF INTESTINAL RINGS IN *C. elegans* BY A FLUORESCENT APICAL JUNCTION REPORTER

For understanding the mechanical coupling of the cytoplasmic intermediate filament cytoskeleton in the intestine, a detailed characterization of the spatial arrangement of the CeAJ is crucial. Using fluorescently labeled components of the CeAJ intermediate filament attachment sites can be easily outlined. The example shown in Fig. 2A and B presents the fluorescence of an mCherry-labeled reporter for the CeAJ component DLG-1 (*C. elegans* homologue of the *Drosophila melanogaster* tumor suppressor gene discs large) revealing a ladder-type pattern in the intestine (Bossinger, Klebes, Segbert, Theres, & Knust, 2001; Firestein & Rongo, 2001; McMahon, Legouis, Vonesch, & Labouesse, 2001). Since its presence is not restricted to the intestine (Fig. 2A), fluorescence signals outside of the pharynx, intestine, and hindgut were removed to prepare Fig. 2A'. In this cropped image, the fluorescence signal in the ints is much better visible. While the first int consists of four cells, all others are made up of two cells each. They are referred to as int1 to int9 from anterior to posterior (Sulston, Schierenberg, White, & Thomson, 1983). Careful inspection shows that (i) the rings are twisted from anterior to posterior with respect to each other in a clockwise direction and (ii) not all half rings are in register with the largest stagger in the middle of the worm. These properties are reason for the characteristic ladder pattern (see also Hermann, Leung, & Priess, 2000; Leung, Hermann, & Priess, 1999). The high-magnification images in Fig. 2B and B' highlight the resulting arrangement of the DLG-1::mCherry-labeled CeAJ in ints6–8. The simplified 3D

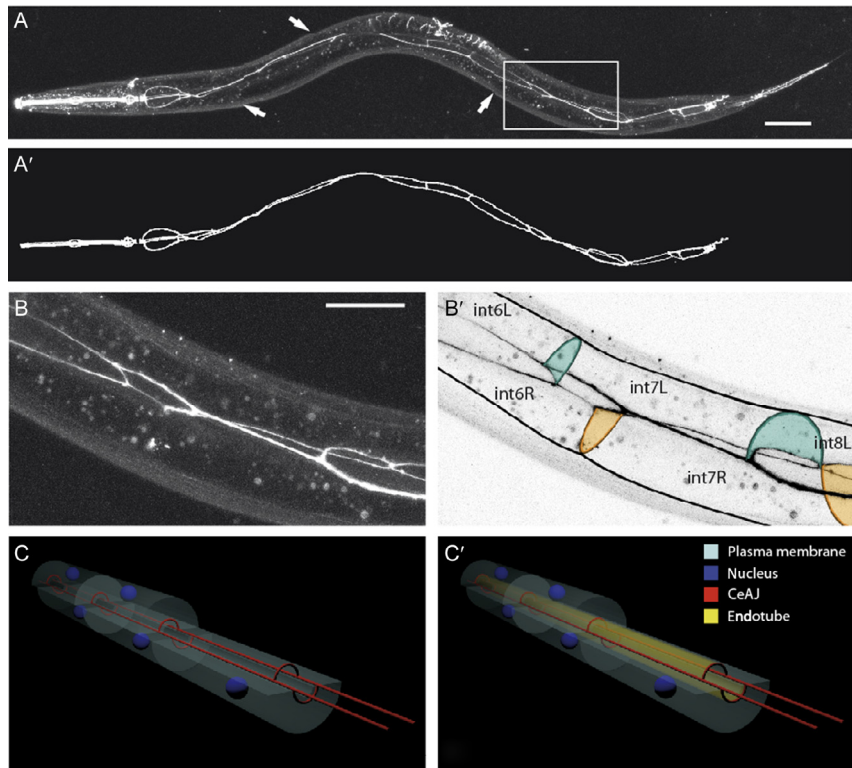


Figure 2 Detection and modeling of the intermediate filament-associated apical cell contacts in the *C. elegans* intestine. (A) Composite micrograph depicting the fluorescence of the CeAJ marker DLG-1::mCherry in the intestine of an L4 *C. elegans* larva as a single-projection view of stitched images. Note that slight movements of the worm resulted in misalignments at borders of image stacks (arrows). Since DLG-1::mCherry is not restricted to the intestine but is also detectable in other tissues including pharynx, rectum, seam cells, hypodermis, spermatheca, and vulva, only focal planes 6–16 of the entire stack of 20 focal planes are shown to improve visualization of the intestinal fluorescence. Panel (A') shows a cropped version of the micrograph in A to further alleviate examination of the intestinal fluorescence pattern (see also corresponding animation in Movie 1 (<http://dx.doi.org/10.1016/bs.mie.2015.08.030>)). (B) High magnification taken from A (boxed area) of a region encompassing int-6 to int-8. Details of the typical ladder pattern can be seen, which are caused by the staggered and clockwise twisted arrangement of the intestinal cells. Panel (B') shows an inverse version of B and also includes the position of the basolateral cell borders, which were drawn manually with the help of simultaneously recorded phase-contrast images (not shown). Panels (C) and (C') Simplified 3D reconstructions of part of the intestine depicting the CeAJ without (C) and with the attached intermediate filament-rich endotube (C'). The corresponding animation in Movie 2 (<http://dx.doi.org/10.1016/bs.mie.2015.08.030>) highlights further details. Scale bars: 50 μm in A (same magnification in A') and 25 μm in B (same magnification in B').

reconstructions in Fig. 2C and C' further demonstrate the CeAJ localization with respect to the cell body and depict, how it serves as an attachment site for the circumferential intermediate filament-rich endotube.

3.1 Confocal Laser Scanning Microscopy of Worms

Viable reporter worms are immobilized on glass slides for high-resolution confocal laser scanning fluorescence microscopy. To record the fluorescence in entire worms, multiple image stacks have to be prepared, assembled, and stitched. Small movements of the animals may pose problems (arrows in Fig. 2A). Imaging parameters have to be adjusted to the intensity and distribution of the reporter construct used. Multiple options are available for 3D reconstruction and visualization.

Materials

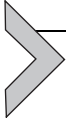
- *C. elegans* strain BJ246 *Is[dlg-1p::dlg-1::mcherry]* (kindly provided by Dr. Andrea Hutterer)

Equipment

- Confocal laser scanning fluorescence microscope (e.g., LSM710 Duo, Carl Zeiss) equipped with a helium–neon laser
- 63× Objective (e.g., Objective Plan-Apochromat 63×/1.40 Oil DIC M27, Carl Zeiss)
- Fiji 1.4 software (National Institutes of Health)
- Amira 5.4 software (Visage Imaging)
- Blender 2.73 (Blender Foundation)

Methods

1. Transfer viable L4 larvae as described in Section 2 into a drop of PBS containing 1 mM Levamisole on a microscope slide.
2. Mount prepared sample on the microscope stage.
3. Detect fluorescence of DLG-1::mCherry with the 543 nm line of the helium–neon laser and set laser intensity to 50%. Monitor the emitted light between 592 and 722 nm with 1.72 airy units. Acquire images in multiple focal planes with an image size of 1024 × 1024 pixel (pixel size 0.13 μm) and record with a grayscale range of 16-bit using a dwell time of 6.3 μs for each pixel.
4. Stitch images using the ZEN software (Carl Zeiss) or any other available software (e.g., Fiji) to obtain a single-image file of the entire worm.
5. Fiji software can be used for image projection and Amira software for 3D reconstruction of the fluorescent signal. For preparing a 3D model of the intestine, use the open-source 3D computer graphics software Blender.



4. DISSECTION OF INTESTINES AND VITALITY TESTING

Tissue mechanics are dependent on the functioning of all cellular components. It is therefore critical to prepare viable intestinal tissue and to assess its functionality. With comparatively little experience, viable intestines can be prepared with this simple procedure. We prefer to use L4 larvae because they can be easily identified in the dissection stereo microscope. In addition, the well-defined L4 stage is rather short (~ 10 h at 22°C) and thereby improves comparability between different worms. It is important to handle the dissected intestine with utmost care to avoid local damage, which would be detrimental to mechanical measurements.

Materials

- Viable L4 larvae
- Coverslip
- Leibovitz's L-15 medium liquid with GlutaMAX™-I (Life Technologies, cat no. 31415-029) supplemented with 10% fetal calf serum (FCS; Life Technologies, cat no. 10270-106) and osmolarity adjusted to 350 ± 5 mOsm with 60% sucrose (Sigma-Aldrich, cat no. S9379) using an osmometer
- Worm pick
- Scalpel

Equipment

- Stereo microscope (e.g., BMS 141 Bino Zoom; Breukhoven B.V.)
- Osmometer (Osmomat 030, Gonotec)

Methods

1. Transfer L4 larva with the worm pick into a drop of medium on a coverslip.
2. Cut the larva at the pharynx just anterior of the posterior bulb using a sharp scalpel.
3. A large part of the intestine will be pushed out from the body cavity because of the high internal pressure. In most instances, the gonads will be squeezed out at the same time. Both remain attached to the body of the worm.
4. Worms can be stored until use (see below).

4.1 Viability Testing of the Dissected Intestine

It is known that the stressed intestine elicits a fluorescent wave from the anterior to the posterior preceding cell death (Coburn et al., 2013; Coburn & Gems, 2013). This phenomenon is explained by massive release

of fluorescence from autofluorescent intestinal granules. These granules are known to be lysosome-related organelles, which contain a glycosylated form of anthranilic acid, a blue fluorophore responsible for the blue fluorescence emitted by the intestinal granules. The fluorescent wave is induced by the calcium-dependent calpain–cathepsin necrotic cell death cascade and is transmitted to adjacent posterior intestinal cells via INX-16 channels. The presence of characteristic autofluorescent granules can therefore be taken as an indication of cell viability. [Figure 3](#) presents fluorescence recordings of dissected intestines immediately after preparation and after 2 h of storage in cell culture medium. In both situations, multiple distinct autofluorescent granules are seen in the isolated intestines at the beginning of the sequence identical to the *in situ* situation ([Coburn et al., 2013](#); [Coburn & Gems, 2013](#)).

Upon repeated irradiation for imaging, however, granular fluorescence disappears and is substituted by a diffuse cytoplasmic fluorescence. These changes are propagated from cell to cell in an anterior-to-posterior direction as is typical for the fluorescent wave ([Fig. 3](#)). We interpret this as a stress reaction to the repeated radiation. Extended storage increases radiation sensitivity (compare [Fig. 3A](#) with [B](#)). Note, however, that appearance of the fluorescent wave is not directly linked to cell death. Instead, another kind of granular fluorescence appears within approximately 15 min. It is not known if these novel granular structures are newly emerging intestinal granules formed through processes such as the endocytosis of substances from the cell culture medium ([Bossinger, Wiegner, & Schierenberg, 1996](#)), other types of vesicles or nonvesicular aggregates. After a lag period, fluorescence is completely lost coinciding with uptake of trypan blue as a definite sign of cell death ([Fig. 4](#)). The lag period may last for more than 30 min in the freshly prepared intestine but may be as short as 5 min after storage ([Fig. 3A](#) and [B](#)). Taken together, we recommend to only use intestines with typical autofluorescent granules for mechanical measurements and to keep irradiation at a minimum.

Materials

- Dissected intestines (see previous section)
- Microscope slides
- Leibovitz's L-15 medium
- 0.4% Trypan blue solution (Sigma-Aldrich, cat no. 93595-50ML)

Equipment

- Fluorescence microscope (e.g., Zeiss ApoTome 2, Carl Zeiss)
- 20× Objective (e.g., Plan-Apochromat 20×/0.8 M27, Carl Zeiss)

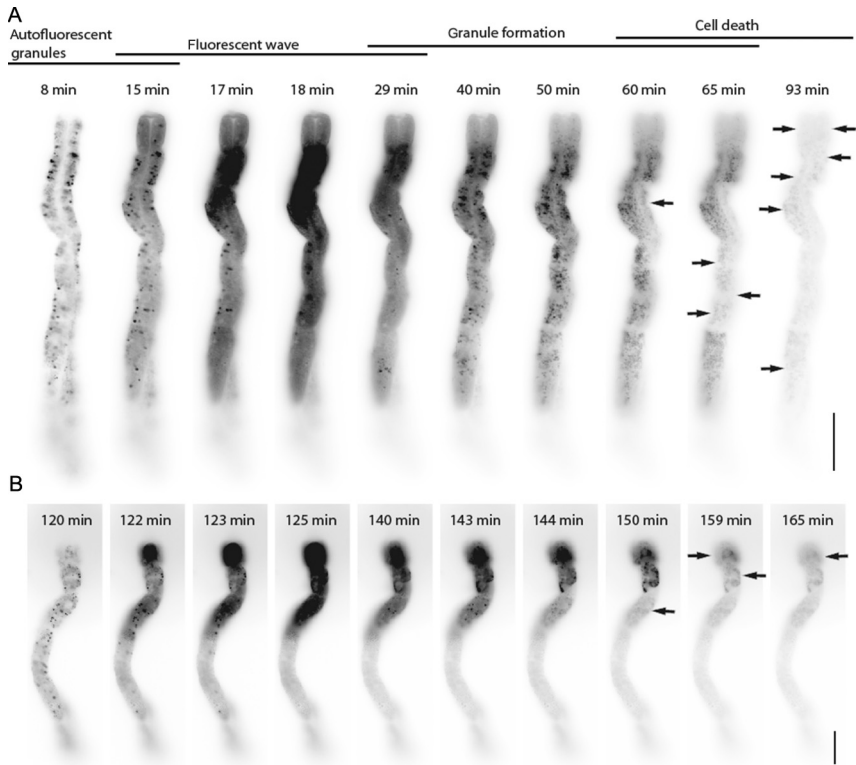


Figure 3 Induction of a fluorescent wave in dissected intestines. The images show fluorescence recordings (grayscale inverted) of an intestine starting either 8 or 120 min after dissection (A and B, respectively). The corresponding complete time series are provided in Movies 3 and 4 (<http://dx.doi.org/10.1016/bs.mie.2015.08.030>). Note the characteristic autofluorescent intestinal granules in the cytoplasm at the beginning of both time series. The autofluorescence of the granules disappears giving rise to increased and diffuse fluorescence. This event is propagated from cell to cell in anterior-to-posterior direction and is referred to as the fluorescent wave. It is followed by appearance of another kind of granular fluorescence (granule formation) and subsequent complete loss of fluorescence upon cell death (arrows). Note that even after 120 min of storage in cell culture medium autofluorescent granules are still clearly visible at the beginning of the recording indicating viability. Induction of the fluorescent wave and cell death, however, occur much more rapidly. Scale bars: 50 μm .

Methods

1. Transfer the dissected worms and adhering internal organs to another drop of medium onto a microscope slide.
2. Record cytoplasmic granular fluorescence using the DAPI filter set.
3. Monitor fluorescence at 30 s intervals.

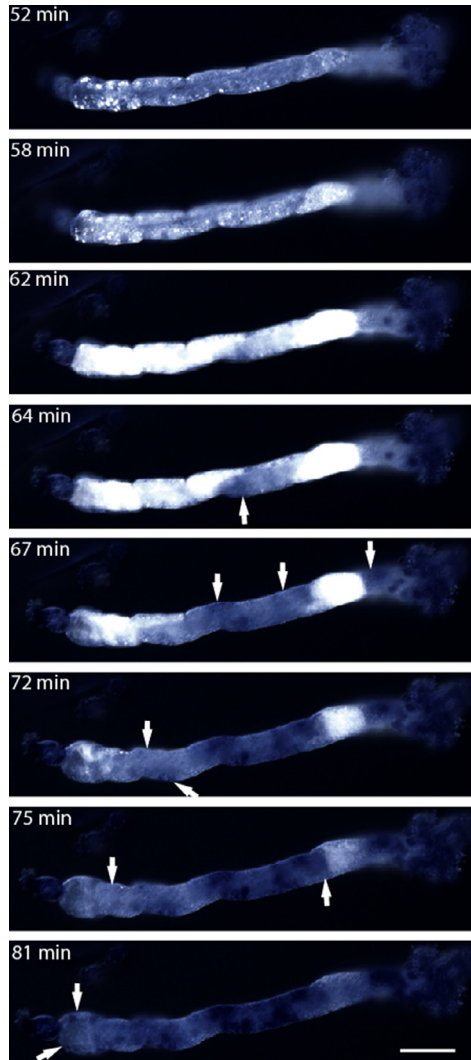


Figure 4 Monitoring cell death by trypan blue staining (dark blue) in dissected intestines. The images are overlays of the phase contrast and fluorescence micrographs in a dissected intestine. The intestine was stored for 52 min in culture medium before recording. The images are taken from a time-lapse recording that is presented in Movie 5 (<http://dx.doi.org/10.1016/bs.mie.2015.08.030>). Note that a fluorescent wave (white) is initiated at 58 min and that loss of fluorescence coincides with uptake of trypan blue into dying cells (arrows). Scale bar: 50 μm .

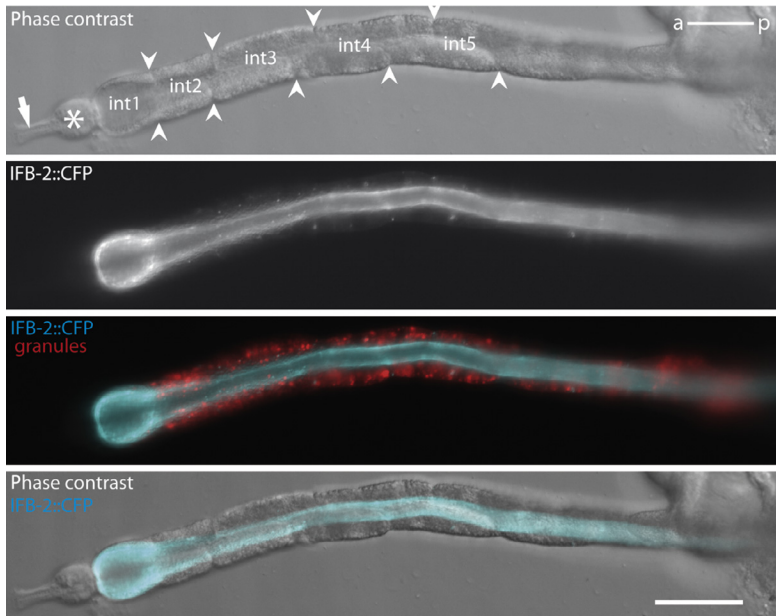
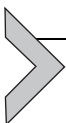


Figure 5 IFB-2::CFP fluorescence in a viable dissected intestine of reporter strain BJ49. Top: phase contrast. Arrow, pharyngeal isthmus; asterisk, terminal pharyngeal bulb; arrowheads, cell borders of intestinal cells between the intestinal rings int1, int2, int3, int4, and int5. Upper middle: corresponding fluorescence recording of IFB-2::CFP. Lower middle: overlay of IFB-2::CFP fluorescence (cyan) and autofluorescent intestinal granules (false red color), which indicate full vitality of the dissected intestine. Bottom: overlay of phase contrast and IFB-2::CFP fluorescence. Note that the distribution of IFB-2::CFP in the dissected intestine is comparable to its distribution in a living L4 larva (Fig. 1). Scale bar: 50 μ m.

4. To check for cell death, add equal volume of 0.4% trypan blue.

The above method can be used to assess vitality in dissected intestines that produce fluorescent reporters such as those shown in Figs. 1 and 2. Figure 5 shows normal-appearing intestinal granules in the dissected intestine of an IFB-2::CFP reporter strain. The fluorescent fusion protein localizes specifically to the periluminal domain as seen in the intact worm (Fig. 1).



5. EXPERIMENTAL SETUP FOR MICROPIPETTE MEASUREMENTS

Micropipettes are well-established tools for mechanical probing (Evans, 1989; Mitchison & Swann, 1954; Needham, 1993). Careful

preparation of micropipettes is essential for high-precision measurements. They have to be tailored to fully attach to the isolated intestine without any leakage and without damaging the brittle cells. The setup for the dual pipette assay needs to be calibrated for each new pipette and needs to be readjusted in between measurements (Ligezowska et al., 2011).

5.1 Forging of Pipettes

Materials

- Borosilicate glass capillaries, 1 mm outer and 0.5 mm inner diameter (Hilgenberg GmbH)

Equipment

- A microforge (own fabrication) comprising (i) a heating filament made of platinum with a drop of low-melting glass solder attached, (ii) a well-regulated current source, (iii) a mechanical micromanipulator for micro-needle maneuvering, and (iv) a stereo microscope (Zhelev, Needham, & Hochmuth, 1994)
- Micropipette puller P-97 Flaming Brown (Sutter Instrument Corporation)

Methods

1. With the help of the micropipette puller, borosilicate glass capillaries are pulled into microneedles with an inner diameter of approximately 2–10 μm using the following settings: heat 551, pull 0, velocity 140, time 200, and pressure 500. Please note that parameters have to be adjusted to your specific instrumentation and lab conditions. The manufactured microneedles are very thin. Handle with care.
2. To obtain a flat and axisymmetric tip of 2–10 μm inner diameter, the microneedle is opened at the end using the microforge. Heat the drop of glass solder slightly above melting temperature. Position the microneedle near the molten drop. Immerse microneedle horizontally into the fluid drop until the tip reaches the desired inner diameter. Let the solder glass cool down. Upon retraction, the microneedle breaks at the surface of the now solid drop of glass. Adjusting temperature and judging pipette diameter during insertion require a bit of experience.
3. The tip of the resulting micropipette is smoothed by bringing it close to the heating wire of the microforge without contacting it directly.
4. Forged micropipettes can be stored in an upright position and dust-free environment until use.

5.2 Calibrating Pipette Setup

Materials

- Silica microspheres ($d = 1.53 \mu\text{m}$, Polysciences, Inc., cat no. 24327-15)
- Leibovitz's L-15 medium

Equipment

- Micropipette flushing needle MicroFil 28 g, 97 mm (cat no. MicroFil MF28G-5, World Precision)
- Bright field light microscope (e.g., Axiovert 200, Carl Zeiss)
- CCD camera (e.g., Sensicam QE, PCO)
- Three-axis water hydraulic fine micromanipulator (e.g., MHW-3 and MX-35A, Narishige Co.)
- A hydraulic pressure control system (own fabrication)
- Culture chamber (own fabrication; 3 mm high glass chamber with a total volume of 2 ml and openings on both sides for pipette access)
- Syringes
- Syringe filter units (Merck Millipore Ltd., cat no. SLGP033RS)
- Tubing and luers
- Pipette holders

Methods

The experimental setup described below is shown schematically in [Fig. 6](#).

1. Install the hydraulic pressure control system consisting of an adjustable water reservoir attached to a 1.6-m long vertical track driven by a geared DC motor (for details, see [Dieluweit et al., 2010](#)) and connect the water reservoir to a pipette holder through a plastic tube. Attach the pipette holder to the three-axis hydraulic micromanipulator.
2. Connect the second pipette holder to a syringe and attach it to the second three-axis hydraulic micromanipulator.
3. Fill both systems with water and ensure that absolutely no air bubbles remain in the system.
4. Fill the micropipettes with medium using a syringe with a syringe filter using a micropipette flushing needle and mount the micropipettes onto the pipette holders. Press some fluid out of each pipette to remove remaining air.
5. Carefully insert the micropipettes laterally into the culture chamber and position them above the sample using the micromanipulators.
6. For calibrating the stretching pipette, adjust the height of the water reservoir and identify the position where no net flow in or out the stretching micropipette is observed. This is accomplished by monitoring the movement of beads that are dispersed in the medium. Even tiny air

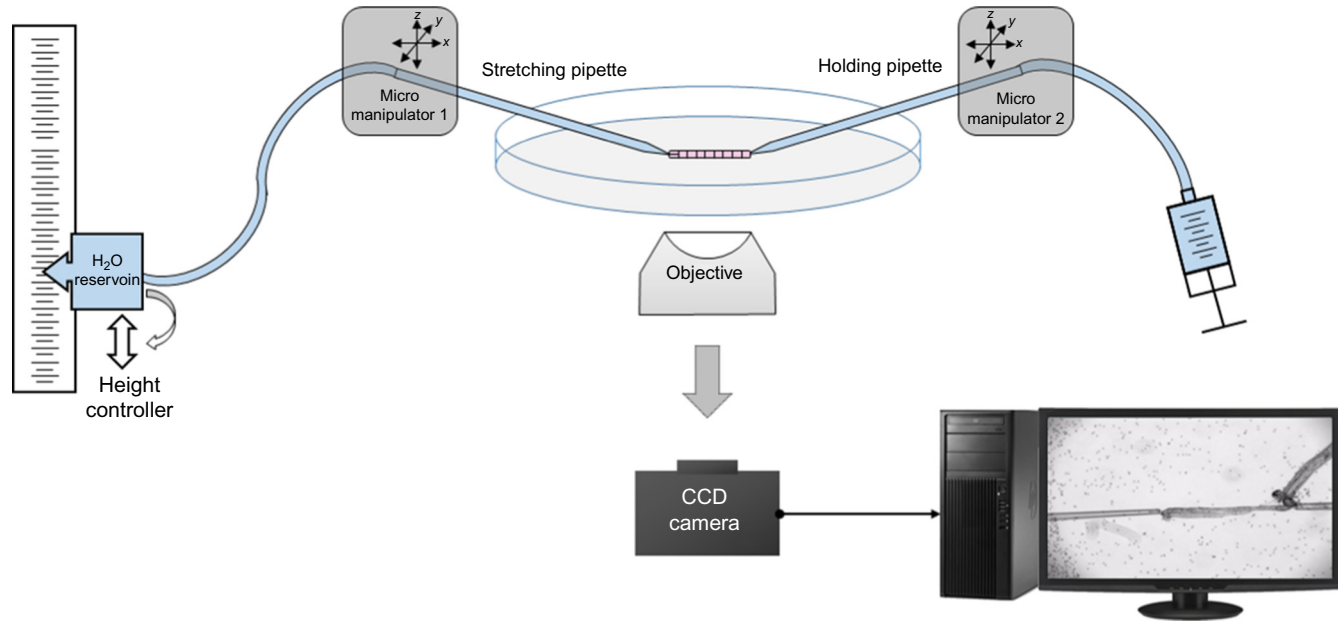


Figure 6 Scheme of experimental setup to measure viscoelasticity of dissected intestines using micropipettes. The dissected intestine is placed in a culture chamber with cell culture medium. With the help of micromanipulators, the posterior end close to the remains of the worm is attached to a holding pipette and the anterior end to a stretching pipette. The latter is connected to a height-adjustable water reservoir for precisely regulating pressure. The intestine is viewed from below with an inverted microscope. Images are recorded with a CCD camera.

bubbles in the system result in unstable zero pressure. Set this position as zero pressure position. Knowing camera pixel size, inner diameter can be calculated from phase-contrast images before experimental start.

5.3 Analysis of Intestinal Mechanics

The following paragraph describes a typical experiment to test the viscoelastic properties of the dissected intestine. Figure 7 illustrates a regimen of repeated stretching experiments at the same force and incrementally increasing forces.

Materials

- Dissected *C. elegans* intestine (section 4)
- Silica microspheres ($d = 1.53 \mu\text{m}$, cat no. 24327-15, Polysciences, Inc.)
- Leibovitz's L-15 medium

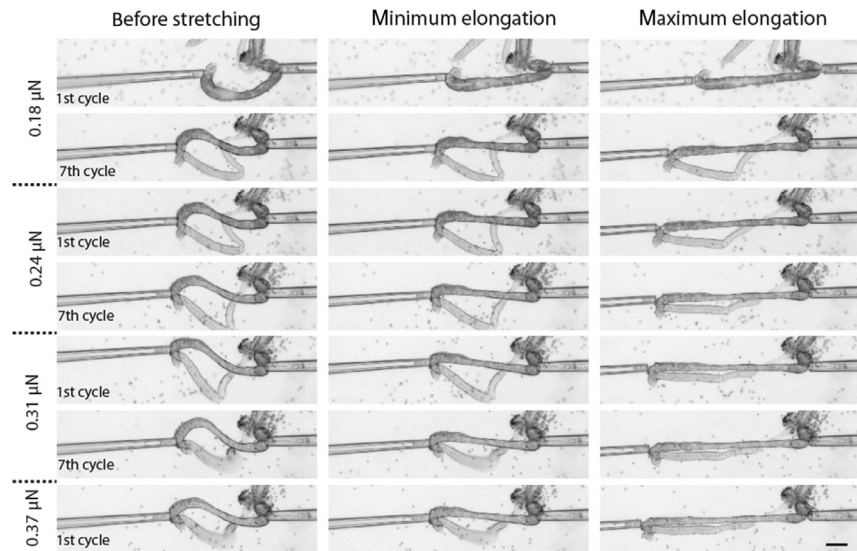


Figure 7 Recording of repeated and incrementally increasing stretching of a dissected intestine. The phase-contrast images are taken from an experiment performed on a single intestine. The stretching pipette (inner diameter $8.9 \mu\text{m}$) is to the left, the holding pipette to the right. Parts of the attached worm can be seen next to the holding pipette, and part of the pharynx can be seen located at the left in front of the first intestinal ring. In addition, the gonads, which were extruded together with the intestine, are also visible in the background. To calibrate the suction pressure and to assess that the pipettes are tightly attached to the intestine, beads are used (black dots). Stretching resulted in elongation, which was increasing with repeated stretching and with elevating suction pressure. Note that intestinal length is reduced between cycles but does not recover completely. The entire image series is provided in Movie 6 (<http://dx.doi.org/10.1016/bs.mie.2015.08.030>). Scale bar: $50 \mu\text{m}$.

Equipment

- Culture chamber (details in 5.2)
- Fluorescence microscope (Axiovert 200, Carl Zeiss)

Methods

1. Transfer dissected intestines with adhering internal organs and the remaining worm into another drop of medium in the culture chamber. Disperse a few indicator beads into the medium.
2. Mount the culture chamber onto the microscope stage and calibrate the stretching pipette (5.2). Afterward, the calibrated stretching micropipette should not be moved vertically any more.
3. Grab the dissected intestine with the holding pipette on the posterior end by aspiration and attach the stretching pipette to the anterior end. Take care of proper sealing.
4. Set the desired aspiration force of the stretching pipette by adjusting the height of the water reservoir. By calculating the difference between the adjusted position and position 0, the aspiration pressure can be calculated using Pascal's law $\Delta P = \rho g \Delta h$, where ΔP is the aspiration pressure, ρ is the fluid density, g is the earth's gravitational acceleration, and Δh is the height difference between position 0 and the adjusted position. Aspiration force F_{Asp} can be calculated according to $F_{\text{Asp}} = \pi R^2 \Delta P$ with R being the inner radius of the stretching pipette and ΔP the aspiration pressure.
5. Adjust the position of the holding pipette without stretching the intestine until both pipettes are aligned along the same axis within the focal plane of the microscope.
6. Start the recording of the microscopic images and stretch the intestine by moving the stretching pipette slowly away from the holding pipette.
7. Stretch the intestine until it detaches from the stretching pipette and document the whole-stretching process for additional time after detachment depending on scientific question.
8. Record epifluorescence and phase-contrast images during stretching process.

Dissected intestines of *C. elegans* strains, in which intermediate filaments are fluorescently labeled, are highly suitable to study mechanical stress-dependent behavior during micropipette-dependent stretching. Figure 8 presents a combination of fluorescence and bright field recordings of a dissected L4 intestine of strain BJ49, which expresses an IFB-2::CFP reporter. Upon stretching, the intestinal endotube shows a similar viscoelastic behavior as the stretched tissue.

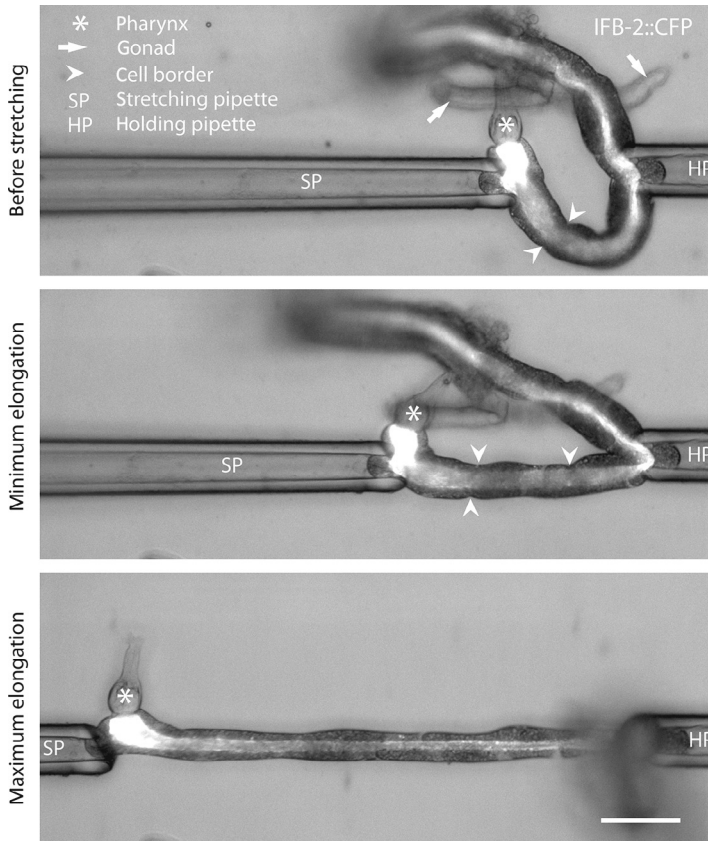


Figure 8 Coordinated stretching of the intermediate filament-rich endotube and cells of a dissected intestine. The intestine was prepared from an IFB-2::CFP reporter worm of strain BJ49. The combined fluorescence and phase-contrast images show that controlled micropipette stretching elongates the intermediate filament system in conjunction with the intestine without any visible damage. Asterisk, pharyngeal bulb; arrowheads, cell borders; SP, stretching pipette; HP, holding pipette. Scale bar: 50 μm .

To estimate the mechanical contribution of the intermediate filament-rich endotube to tissue integrity, the pharynx of a dissected intestine was cut off in order to deliberately generate a weak point (asterisk in Fig. 9). Figure 9 shows the IFB-2::CFP fluorescence during repeated stretches of the dissected intestine at high-aspiration force. The dissected intestine experienced a particularly high degree of deformation during stretching at the attachment positions of the pipettes. Cells weakened at these positions. Even when their cytoplasm was sucked into the pipettes, the intermediate filament system remained fully intact (arrow, arrowhead).

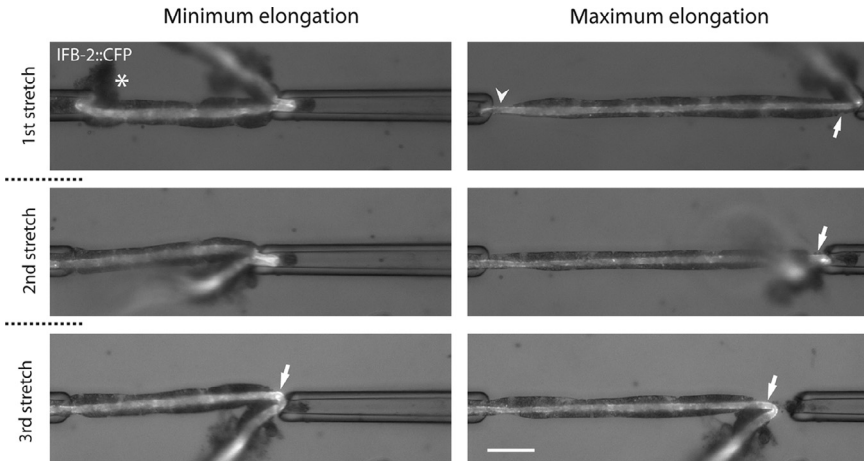
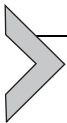


Figure 9 Maintenance of the intermediate filament-rich endotube after cell disruption. Cutting off the pharynx induces a weak point into the intestinal tissue architecture leading to substantial damage of the first intestinal ring (asterisk). Note that during the first stretch cycle cellular remains of the first intestinal ring are ripped off by the left pipette, but the endotube is not disrupted (arrowhead). At the attachment point of the right pipette parts of the cells including the endotube are aspirated into the pipette. During stretching, damages to the attached cells are observed up to the point, where they are peeled off uncovering the intermediate filament-rich endotube (arrows). Note that the endotube shows no visible signs of damage. Scale bar: 50 μm .



6. OUTLOOK

The examples presented highlight the advantages of the dissected *C. elegans* intestine as a model system for the examination of tissue mechanics and reveal its unique properties. They further highlight the extreme mechanical resilience of the *C. elegans* intermediate filament system, which withstands forces up to 1 μN and can be stretched to more than 150% without rupture even when the rest of the cell is pulled away. Our data further demonstrate that the intestine does not fully resume its original length after stretching. Taken together, we conclude that both an elastic and a plastic component determine intestinal mechanics. These observations considerably extend the report of [Beriault et al. \(2012\)](#), who imaged the keratin cytoskeleton in cultured cells upon extensive stretching and the work by [Fois et al. \(2013\)](#), [Hecht et al. \(2012\)](#), and [Felder et al. \(2008\)](#), who examined biochemical and morphological alterations of the keratin cytoskeleton during and after stretching. Our observations furthermore demonstrate that very stable and resilient cell–cell junctions control the organization of the

C. elegans intermediate filament system, since dissociation at cell–cell borders did not occur. Our setup offers an ideal system to study, how and to which degree the intermediate filament system and its associated structures contribute to the mechanical properties of the intestine. It may help to characterize and identify auxiliary and other systems that contribute to the unique mechanical resilience of the *C. elegans* intestine. The use of genetically modified worms will greatly help in this endeavor. Mutants are freely available (e.g., *Caenorhabditis* Genetics Center), or gene expression can be down-regulated through RNA interference (RNAi) by feeding (using, e.g., the clones available in the Ahringer RNAi-library (Geneservice)). Alternatively, drugs can be used to selectively disrupt cytoskeletal components or signaling pathways. The experimental setup allows monitoring the localization of components of the CeAJ and the apical cytoskeleton using fluorescent reporter strains during mechanical manipulation. The described experimental system also shows promise for examining the mechanosensory response of the intestinal epithelium. Combining stretching experiments with local measurements of enzyme activity, ion concentration and pH will further expand our understanding of the complex organization and regulation of the intermediate filament cytoskeleton and to describe a biological function of the different cell adhesion complexes (Bossinger et al., 2001; Pásti & Labouesse, 2014; Piliipiuk, Lefebvre, Wiesenfahrt, Legouis, & Bossinger, 2009; Waaijers, Ramalho, Koorman, Kruse, & Boxem, 2015).

ACKNOWLEDGMENTS

This work was supported by a scholarship from the Jürgen Manchot-Stiftung to O.J. and by grants from the German Research Council to R.M. (ME 1458/6-3), O.B. (BO 1061/11-3), and R.L. (LE566 14-3).

REFERENCES

- Beil, M., Micoulet, A., von Wichert, G., Paschke, S., Walther, P., Omary, M. B., et al. (2003). Sphingosylphosphorylcholine regulates keratin network architecture and visco-elastic properties of human cancer cells. *Nature Cell Biology*, 5, 803–811.
- Beriault, D. R., Haddad, O., McCuaig, J. V., Robinson, Z. J., Russell, D., Lane, E. B., et al. (2012). The mechanical behavior of mutant K14-R125P keratin bundles and networks in NEB-1 keratinocytes. *PLoS One*, 7, e31320.
- Bossinger, O., Fukushige, T., Claeys, M., Borgonie, G., & McGhee, J. D. (2004). The apical disposition of the *Caenorhabditis elegans* intestinal terminal web is maintained by LET-413. *Developmental Biology*, 268, 448–456.
- Bossinger, O., Klebes, A., Segbert, C., Theres, C., & Knust, E. (2001). Zonula adherens formation in *Caenorhabditis elegans* requires *dlg-1*, the homologue of the *Drosophila* gene discs large. *Developmental Biology*, 230, 29–42.

- Bossinger, O., Wiegner, O., & Schierenberg, E. (1996). Embryonic gut differentiation in nematodes: Endocytosis of macromolecules and its experimental inhibition. *Roux's Archives of Developmental Biology*, *205*, 494–497.
- Brown, M. J., Hallam, J. A., Colucci-Guyon, E., & Shaw, S. (2001). Rigidity of circulating lymphocytes is primarily conferred by vimentin intermediate filaments. *The Journal of Immunology*, *166*, 6640–6646.
- Carberry, K., Wiesenfahrt, T., Geisler, F., Stöcker, S., Gerhardus, H., Überbach, D., et al. (2012). The novel intestinal filament organizer IFO-1 contributes to epithelial integrity in concert with ERM-1 and DLG-1. *Development*, *139*, 1851–1862.
- Carberry, K., Wiesenfahrt, T., Windoffer, R., Bossinger, O., & Leube, R. E. (2009). Intermediate filaments in *Caenorhabditis elegans*. *Cell Motility and the Cytoskeleton*, *66*, 852–864.
- Coburn, C., Allman, E., Mahanti, P., Benedetto, A., Cabreiro, F., Pincus, Z., et al. (2013). Anthranilate fluorescence marks a calcium-propagated necrotic wave that promotes organismal death in *C. elegans*. *PLoS Biology*, *11*, e1001613.
- Coburn, C., & Gems, D. (2013). The mysterious case of the *C. elegans* gut granule: Death fluorescence, anthranilic acid and the kynurenine pathway. *Frontiers in Genetics*, *4*, 151.
- Dieluweit, S., Csiszár, A., Rubner, W., Fleischhauer, J., Houben, S., & Merkel, R. (2010). Mechanical properties of bare and protein-coated giant unilamellar phospholipid vesicles. A comparative study of micropipet aspiration and atomic force microscopy. *Langmuir*, *26*, 11041–11049.
- Dodemont, H., Riemer, D., Ledger, N., & Weber, K. (1994). Eight genes and alternative RNA processing pathways generate an unexpectedly large diversity of cytoplasmic intermediate filament proteins in the nematode *Caenorhabditis elegans*. *The EMBO Journal*, *13*, 2625.
- Eckes, B., Dogic, D., Colucci-Guyon, E., Wang, N., Maniotis, A., Ingber, D., et al. (1998). Impaired mechanical stability, migration and contractile capacity in vimentin-deficient fibroblasts. *Journal of Cell Science*, *111*, 1897–1907.
- Evans, E. A. (1989). Structure and deformation properties of red blood cells: Concepts and quantitative methods. *Methods in Enzymology*, *173*, 3–35.
- Felder, E., Siebenbrunner, M., Busch, T., Fois, G., Miklavc, P., Walther, P., et al. (2008). Mechanical strain of alveolar type II cells in culture: Changes in the transcellular cytokeratin network and adaptations. *American Journal of Physiology. Lung Cellular and Molecular Physiology*, *295*, L849–L857.
- Firestein, B. L., & Rongo, C. (2001). DLG-1 is a MAGUK similar to SAP97 and is required for adherens junction formation. *Molecular Biology of the Cell*, *12*(11), 3465–3475.
- Fois, G., Weimer, M., Busch, T., Felder, E. T., Oswald, F., von Wichert, G., et al. (2013). Effects of keratin phosphorylation on the mechanical properties of keratin filaments in living cells. *The FASEB Journal*, *27*, 1322–1329.
- Fudge, D., Russell, D., Beriault, D., Moore, W., Lane, E. B., & Vogl, A. W. (2008). The intermediate filament network in cultured human keratinocytes is remarkably extensible and resilient. *PLoS One*, *3*, e2327.
- Gruenbaum, Y., Lee, K. K., Liu, J., Cohen, M., & Wilson, K. L. (2002). The expression, lamin-dependent localization and RNAi depletion phenotype for emerin in *C. elegans*. *Journal of Cell Science*, *115*, 923–929.
- Hecht, E., Knittel, P., Felder, E., Dietl, P., Mizaikoff, B., & Kranz, C. (2012). Combining atomic force-fluorescence microscopy with a stretching device for analyzing mechanotransduction processes in living cells. *The Analyst*, *137*, 5208.
- Hermann, G. J., Leung, B., & Priess, J. R. (2000). Left-right asymmetry in *C. elegans* intestine organogenesis involves a LIN-12/Notch signaling pathway. *Development*, *127*, 3429–3440.
- Homberg, M., & Magin, T. M. (2014). Beyond expectations: Novel insights into epidermal keratin function and regulation. In K. W. Jeon (Ed.), *International review of cell and*

- molecular biology*: Vol. 311 (pp. 265–306): San-Diego: Academic Press. <http://dx.doi.org/10.1016/b978-0-12-800179-0.00007-6>.
- Hüsken, K., Wiesenfahrt, T., Abraham, C., Windoffer, R., Bossinger, O., & Leube, R. E. (2008). Maintenance of the intestinal tube in *Caenorhabditis elegans*: The role of the intermediate filament protein IFC-2. *Differentiation*, 76, 881–896.
- Janmey, P. A., Euteneuer, U., Traub, P., & Schliwa, M. (1991). Viscoelastic properties of vimentin compared with other filamentous biopolymer networks. *The Journal of Cell Biology*, 113, 155–160.
- Karabinos, A., Schmidt, H., Harborth, J., Schnabel, R., & Weber, K. (2001). Essential roles for four cytoplasmic intermediate filament proteins in *Caenorhabditis elegans* development. *Proceedings of the National Academy of Sciences of the United States of America*, 98, 7863–7868.
- Kreplak, L., Bär, H., Leterrier, J. F., Herrmann, H., & Aebi, U. (2005). Exploring the mechanical behavior of single intermediate filaments. *Journal of Molecular Biology*, 354, 569–577.
- Kröger, C., Loschke, F., Schwarz, N., Windoffer, R., Leube, R. E., & Magin, T. M. (2013). Keratins control intercellular adhesion involving PKC- α -mediated desmoplakin phosphorylation. *The Journal of Cell Biology*, 201, 681–692.
- Leung, B., Hermann, G. J., & Priess, J. R. (1999). Organogenesis of the *Caenorhabditis elegans* intestine. *Developmental Biology*, 216, 114–134.
- Ligezowska, A., Boye, K., Eble, J. A., Hoffmann, B., Klösigen, B., & Merkel, R. (2011). Mechanically enforced bond dissociation reports synergistic influence of Mn^{2+} and Mg^{2+} on the interaction between integrin $\alpha 7 \beta 1$ and invasin. *Journal of Molecular Recognition*, 24, 715–723.
- Lin, Y.-C., Yao, N. Y., Broedersz, C. P., Herrmann, H., MacKintosh, F. C., & Weitz, D. A. (2010). Origins of elasticity in intermediate filament networks. *Physical Review Letters*, 104, 058101. <http://dx.doi.org/10.1103/PhysRevLett.104.058101>.
- Liovic, M., Lee, B., Tomic-Canic, M., D'Alessandro, M., Bolshakov, V. N., & Lane, E. B. (2008). Dual-specificity phosphatases in the hypo-osmotic stress response of keratin-defective epithelial cell lines. *Experimental Cell Research*, 314, 2066–2075.
- Liu, J., Ben-Shahar, T. R., Riemer, D., Treinin, M., Spann, P., Weber, K., et al. (2000). Essential roles for *Caenorhabditis elegans* lamin gene in nuclear organization, cell cycle progression, and spatial organization of nuclear pore complexes. *Molecular Biology of the Cell*, 11, 3937–3947.
- Lulevich, V., Yang, H., Rivkah Isseroff, R., & Liu, G. (2010). Single cell mechanics of keratinocyte cells. *Ultramicroscopy*, 110, 1435–1442.
- McGhee, J. D. (2013). The *Caenorhabditis elegans* intestine. *Wiley Interdisciplinary Reviews: Developmental Biology*, 2, 347–367.
- McMahon, L., Legouis, R., Vonesch, J.-L., & Labouesse, M. (2001). Assembly of *C. elegans* apical junctions involves positioning and compaction by LET-413 and protein aggregation by the MAGUK protein DLG-1. *Journal of Cell Science*, 114, 2265–2277.
- Mitchison, J. M., & Swann, M. M. (1954). The mechanical properties of the cell surface I. The cell elastimeter. *Journal of Experimental Biology*, 31, 443–460.
- Munn, E. A., & Greenwood, C. A. (1984). The occurrence of submicrovillar endotube (modified termina web) and associated cytoskeletal structures in the intestinal epithelia of nematodes. *Philosophical Transactions of the Royal Society of London. Series B, Biological Sciences*, 306, 1–18.
- Needham, D. (1993). Measurement of interbilayer adhesion energies. In N. Duzgunes (Ed.), *Methods in enzymology*: Vol. 220 (pp. 111–129): Oxford: Academic Press. [http://dx.doi.org/10.1016/0076-6879\(93\)20078-h](http://dx.doi.org/10.1016/0076-6879(93)20078-h).
- Pásti, G., & Labouesse, M. (2014). Epithelial junctions, cytoskeleton, and polarity. *WormBook: The Online Review of C. elegans Biology*, 4, 1–35.

- Paust, T., Paschke, S., Beil, M., & Marti, O. (2013). Microrheology of keratin networks in cancer cells. *Physical Biology*, *10*, 065008.
- Pilipiuk, J., Lefebvre, C., Wiesenfahrt, T., Legouis, R., & Bossinger, O. (2009). Increased IP3/Ca²⁺ signaling compensates depletion of LET-413/DLG-1 in *C. elegans* epithelial junction assembly. *Developmental Biology*, *327*, 34–47.
- Plodinec, M., Loparic, M., Suetterlin, R., Herrmann, H., Aebi, U., & Schoenenberger, C.-A. (2011). The nanomechanical properties of rat fibroblasts are modulated by interfering with the vimentin intermediate filament system. *Journal of Structural Biology*, *174*, 476–484.
- Ramms, L., Fabris, G., Windoffer, R., Schwarz, N., Springer, R., Zhou, C., et al. (2013). Keratins as the main component for the mechanical integrity of keratinocytes. *Proceedings of the National Academy of Sciences of the United States of America*, *110*, 18513–18518.
- Rolli, C. G., Seufferlein, T., Kemkemer, R., & Spatz, J. P. (2010). Impact of tumor cell cytoskeleton organization on invasiveness and migration: A microchannel-based approach. *PLoS One*, *5*, e8726.
- Russell, D., Ross, H., & Lane, E. B. (2010). ERK involvement in resistance to apoptosis in keratinocytes with mutant keratin. *Journal of Investigative Dermatology*, *130*, 671–681.
- Seltmann, K., Cheng, F., Wiche, G., Eriksson, J. E., & Magin, T. M. (2015). Keratins stabilize hemidesmosomes through regulation of β 4-integrin turnover. *Journal of Investigative Dermatology*, *135*, 1609–1620. <http://dx.doi.org/10.1038/jid.2015.46>.
- Seltmann, K., Fritsch, A. W., Kas, J. A., & Magin, T. M. (2013). Keratins significantly contribute to cell stiffness and impact invasive behavior. *Proceedings of the National Academy of Sciences of the United States of America*, *110*, 18507–18512.
- Seltmann, K., Roth, W., Kröger, C., Loschke, F., Lederer, M., Hüttelmaier, S., et al. (2013). Keratins mediate localization of hemidesmosomes and repress cell motility. *Journal of Investigative Dermatology*, *133*, 181–190.
- Sivaramakrishnan, S., DeGiulio, J. V., Lorand, L., Goldman, R. D., & Ridge, K. M. (2008). Micromechanical properties of keratin intermediate filament networks. *Proceedings of the National Academy of Sciences of the United States of America*, *105*, 889–894.
- Sulston, J. E., Schierenberg, E., White, J. G., & Thomson, J. N. (1983). The embryonic cell lineage of the nematode *Caenorhabditis elegans*. *Developmental Biology*, *100*, 64–119.
- Waaaijers, S., Ramalho, J. J., Koorman, T., Kruse, E., & Boxem, M. (2015). The *C. elegans* Crumbs family contains a CRB3 homolog and is not essential for viability. *Biology Open*, *4*, 276–284.
- Walter, N., Busch, T., Seufferlein, T., & Spatz, J. P. (2011). Elastic moduli of living epithelial pancreatic cancer cells and their skeletonized keratin intermediate filament network. *Biointerphases*, *6*, 79–85.
- Wang, N., & Stamenović, D. (2000). Contribution of intermediate filaments to cell stiffness, stiffening, and growth. *American Journal of Physiology. Cell Physiology*, *279*, C188–C194.
- Zhang, H., Landmann, F., Zahreddine, H., Rodriguez, D., Koch, M., & Labouesse, M. (2011). A tension-induced mechanotransduction pathway promotes epithelial morphogenesis. *Nature*, *471*, 99–103.
- Zhelev, D. V., Needham, D., & Hochmuth, R. M. (1994). A novel micropipet method for measuring the bending modulus of vesicle membranes. *Biophysical Journal*, *67*, 720–727.